ADVANCED MATERIALS
www.advmat.de

Domain Formations and Pattern Transitions via Instabilities in Soft Heterogeneous Materials

*Jian Li, Tarkes Dora Pallicity, Viacheslav Slesarenko, Artemii Goshkoderia, and Stephan Rudykh**

Experimental observations of domain formations and pattern transitions in soft particulate composites under large deformations are reported herein. The system of stiff inclusions periodically distributed in a soft elastomeric matrix experiences dramatic microstructure changes upon the development of elastic instabilities. In the experiments, the formation of microstructures with antisymmetric domains and their geometrically tailored evolution into a variety of patterns of cooperative particle rearrangements are observed. Through experimental and numerical analyses, it is shown that these patterns can be tailored by tuning the initial microstructural periodicity and concentration of the inclusions. Thus, these fully determined new patterns can be achieved by fine tuning of the initial microstructure.

Soft materials can develop large deformations in response to various external stimuli, such as mechanical loading,[1] electrical[2,3] and magnetic fields,[4–6] heat,[7,8] and light,[9,10] thus providing rich opportunities for the design of responsive and reconfigurable functional materials with novel and unusual properties.[11–13] Moreover, the performance of soft materials can be further empowered via the instability phenomenon giving rise to dramatic structural changes.[14] This approach enables diverse applications including flexible electronics,[15–19] optical[20] and acoustic[21–23] switches, auxetic materials,[24] surface pattern control,[25] and soft robotics.[26,27] The instability-induced microstructure transformations discovered in the soft system with periodic voids[28,29] have led to the development of programmable mechanical metamaterials,[30,31] switchable auxetic materials,[32–35] color displayers,[36] wave absorbers,[37–40] and actuators.[41] To predict the onset of elastic instabilities and associated microstructure transformations in soft materials, the nonlinear elasticity framework of small perturbations superimposed on large deformations is employed.[42] Based on the homogenized material response, macroscopic instability or so-called long wave instability can be predicted.[43,44] The macroscopic instability corresponds to a special limit in the Bloch–Floquet analysis[45,46] that allows to detect the onset of instability and corresponding mode at different wavelengths. This approach has been successfully used to theoretically predict instability-induced microstructure transformations in various soft systems that have been realized in experiments.[28,32–35] Furthermore, recent development in advanced material fabrication techniques, such as 3D printing[47] and interference lithography,[48] allows the realization of predesigned soft microstructures at various length scales, and extending applications of these intrinsic pattern transformations in reconfigurable materials.

In this paper, we report our experimental observations of the formation of antisymmetric domain and its geometrically tailored evolution into a variety of patterns with cooperative particle rearrangements in soft composites under large deformations. We study the system of stiff inclusions periodically distributed in a soft elastomeric matrix experiencing dramatic microstructure transformations upon development of elastic instabilities. We experimentally realize the instability-induced modes of transformative microstructures from domain formations to cooperative new patterns of particles rearranged in wavy chains, depending on the initial microstructural periodicity and concentration of the inclusions. The numerical Bloch–Floquet instability analysis is employed to investigate the effect of geometrical parameters and material compositions on the composite buckling behaviors giving rise to the formations of various patterns.

Soft composite samples with stiff circular inclusions periodically distributed in a soft elastomeric matrix were fabricated with an Object Connex 260-3 3D printer. A schematic illustration of the composite microstructure is shown in **Figure 1**a. The geometric parameters are defined through periodicity aspect ratio $\eta = w/h$ and inclusion spacing ratio $\xi = d/h$, where w and h denote the unit cell width and height, respectively, and d is the diameter of the inclusions. The soft matrix was printed in the TangoBlack Plus resin (shear modulus μ_{m} = 0.2 MPa),

J. Li, Dr. T. D. Pallicity,[+] Dr. V. Slesarenko, A. Goshkoderia
Department of Aerospace Engineering
Technion–Israel Institute of Technology
Haifa 32000, Israel
Prof. S. Rudykh
Department of Mechanical Engineering
University of Wisconsin Madison
Madison, WI 53706, USA
E-mail: rudykh@wisc.edu
The ORCID identification number(s) for the author(s) of this article can be found under https://doi.org/10.1002/adma.201807309.
[+]Present address: Institute of Engineering Mechanics (ITM), Chair for Continuum Mechanics, Karlsruhe Institute of Technology (KIT), Karlsruhe, Germany

DOI: 10.1002/adma.201807309

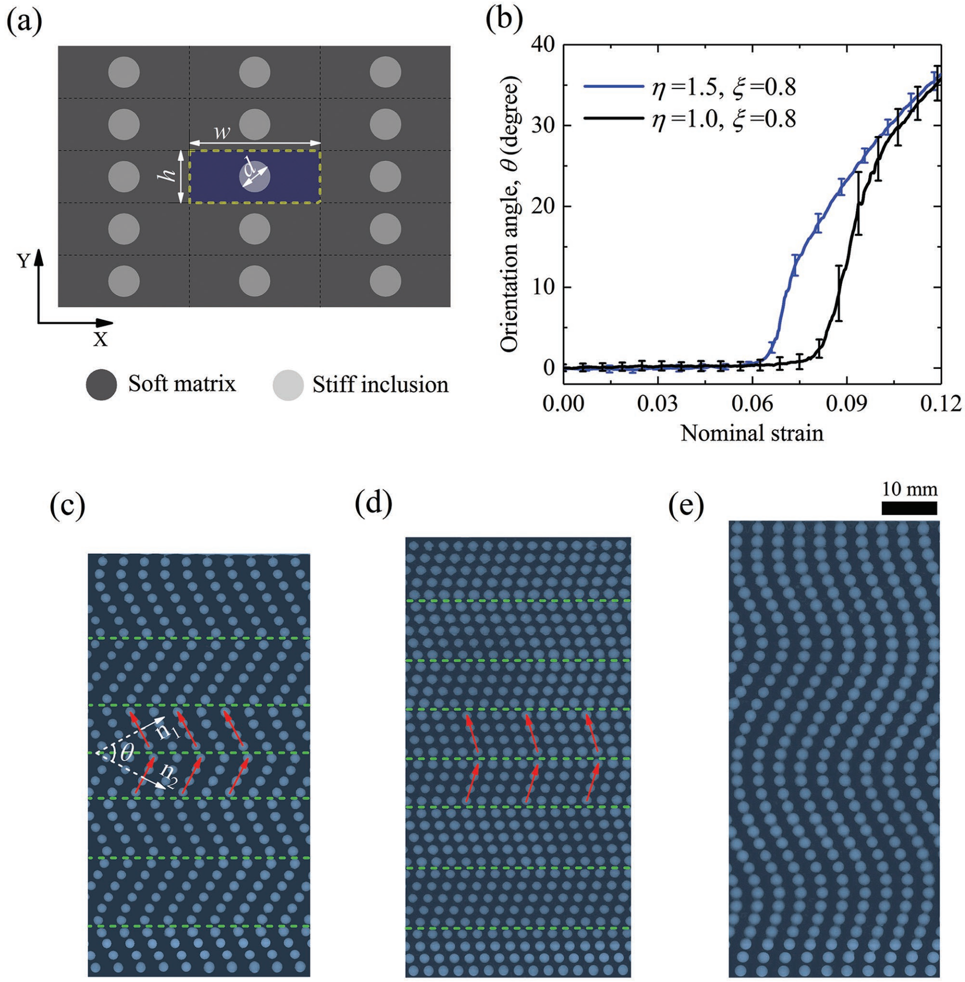

Figure 1. a) Schematic composite microstructure with stiff circular inclusions periodically distributed in a soft matrix, and the primitive unit cell is highlighted in light navy color. b) The dependence of domain orientation angle on the applied strain. Experimental images of instability-induced domain formations c,d) and periodic wavy particle chains e); the results are given for the composites with $\xi = 0.8$, $\eta = 1.5$ c), $\xi = 0.8$, $\eta = 1.0$ d), $\xi = 0.9$, and $\eta = 1.5$ e) at strains $\varepsilon = 0.15$ c), 0.11 d), and 0.08 e).

and the stiff circular inclusions were printed in the VeroWhite resin (shear modulus μ_i = 600 MPa). We first examined the behavior of the soft composites with large spacing ratio and small periodicity aspect ratio, where the domain formations or long wave modes are predicted. In particular, the specimens with $\xi = 0.8$, $\eta = 1.5$; $\xi = 0.8$, $\eta = 1.0$; and $\xi = 0.9$, $\eta = 1.5$ were tested experimentally. Next, the effect of periodicity aspect ratio and the inclusion spacing ratio on the composite behaviors was experimentally investigated separately. Two series of specimens were fabricated: A) the composites with fixed spacing ratio $\xi = 0.8$ and varying periodicity aspect ratio $\eta = 1.5$, 4, 8, 24, and B) the composites with fixed aspect ratio $\eta = 3$ and inclusion spacing ratio $\xi = 0.7$, 0.8, 0.9, 0.95. The in-plane dimensions of the specimens were 60 × 90 mm (width × height), and the out-plane thickness of the specimens was $t = 5$ mm. The unit cell height (defined in Figure 1a) for all specimens was fixed as $h = 2.5$ mm. To diminish the influence of boundary effects on buckling behaviors of the composites, all specimens were printed with a TangoBlack Plus resin boundary layer of 25 mm width.

The uniaxial compression tests were performed using a Shimadzu EZ-LX testing machine. The deformation in the thickness direction was prevented by placing the specimens in a transparent parallel fixture to maintain the plane strain conditions. The specimens were compressed in the Y-direction at a constant velocity of 1 mm min^{-1}. During the test, the compression force and displacement were recorded by the data acquisition system; the deformation processes were captured by the high-resolution charge coupled device (CCD) camera. Multiple samples with identical material properties and geometries were printed and tested to ensure that the observed phenomenon is independent of the individual tests.

Simulations are performed by means of the finite element code (COMSOL 5.2a). The soft matrix and stiff inclusions are modeled as nearly incompressible neo-Hookean materials. The plane-strain conditions are imposed in the simulations. To detect the onset of instabilities in the periodic particulate soft composite and the associated critical strain ε_{cr} and critical wavenumber k_{cr}, we conduct the Bloch–Floquet analysis superimposed on the deformed state.[37,49] The primitive unit cell (as shown in Figure 1a) is constructed, and the corresponding displacement boundary conditions are imposed on the unit cell edges. The analysis is performed in two steps: 1) first, we apply the averaged macroscopic deformation through imposing the corresponding periodic displacement boundary conditions on the unit cell edges to obtain the deformed state; 2) we superimpose the Bloch–Floquet boundary conditions on the unit cell edges and solve the corresponding eigenvalue problem for a range of wavenumbers. These steps are repeated until a nontrivial zero eigenvalue is detected at a certain applied deformation level. Then, the corresponding critical strain and wavenumber are identified. Note that the macroscopic instabilities are detected when $k_{cr} \rightarrow 0$.[46] A more detailed description of the simulations can be found in the Supporting Information.

First, we examine the behavior of the soft composite configurations giving rise to domain formations; these microstructural configurations correspond to the soft composites with large particle spacing ratio and small periodicity aspect ratio. Figure 1c–e shows the instability-induced patterns in soft composites with c) $\xi = 0.8$, $\eta = 1.5$; d) $\xi = 0.8$, $\eta = 1.0$; and e) $\xi = 0.9$, $\eta = 1.5$ at applied strain levels c) $\varepsilon = 0.15$, d) 0.11, and e) 0.08. The corresponding critical strains in the composites are c) $\varepsilon_{cr} = 0.088$, d) 0.089, and e) 0.038, respectively. Figure 1c,d shows that the composites with aspect ratio $\eta = 1.0$, 1.5 (with fixed particle spacing ratio $\xi = 0.8$) form antisymmetric domains upon the development of instabilities. Interestingly, similar domains or twin patterns were also observed in different systems such as martensitic phase transformations,[50,51] liquid crystals,[52,53] nematic elastomers,[54,55] and stiff thin films bonded on a soft substrate.[56–58] The observed domains (marked by the dashed green lines) consist of approximately five unit cells; the particles within the domain align in straight lines with the orientations (or directors) marked by red arrows. The domain orientation changes with the applied deformation as illustrated in Figure 1b showing the experimentally observed domain orientation evolutions. Prior to the onset of instability, the inclusions are aligned in the vertical straight lines corresponding to the zero domain orientation angle. When the applied deformation exceeds the critical strain, the domains start forming, and the orientation angle rapidly increases with an increase in compressive strain. Finally, we note that the increase in particle spacing ratio leads to the transformation of the instability-induced pattern into cooperative particle rearrangements as wavy chains (see Figure 1e for the soft composite with $\eta = 1.5$, $\xi = 0.9$). The period of wavy chains consists of ≈20 inclusions.

To identify the key parameters dictating the instability-induced pattern evolutions, we analyze the soft composite behaviors with varying initial microstructure geometrical parameters. First, we examine the role of the periodicity aspect ratio on the soft composite behavior, while keeping the inclusion spacing ratio fixed. **Figure 2** shows the deformation sequences of the composites with various periodicity aspect ratios at different deformation levels. The results are given for the composites with periodicity aspect ratio $\eta = 1.5$, 4, 8, 24 (from the left to the right columns); the inclusion spacing ratio is fixed $\xi = 0.8$. We observe that the composite microstructure experiences a rapid change upon exceeding the critical strain. For the composite with relatively small periodicity ratio $\eta = 1.5$ (see Figure 2a), we observe that the development of instability results in the stiff inclusions rearranged into antisymmetric domains, similar to the one shown in Figure 1d. We find that the director orientation (denoted by red arrows in Figure. 1c,d) of each domain rotates with further increase in applied deformation. The composites with $\eta = 4$, 8, 24 develop different patterns of periodic wavy chains of particles upon instabilities (see Figure 2b–d). Thus, the instability-induced patterns exhibit a transition from the domain formations to the appearance of wavy patterns. Moreover, we find that the length of the formed wavy chain patterns decreases with the increase in periodicity aspect ratio; for example, the period of wavy chain for the composite with $\eta = 4$ consists of approximately eight inclusions, while the composite with $\eta = 8$ forms a period with approximately five inclusions. Furthermore, we note that the evolution of the instability-induced pattern transformations for the composites with $\eta = 8$, 24 is almost identical (compare Figure 2c,d). This is due to the fact that the interactions between the columns of stiff inclusions become weak in composites with large periodicity aspect ratio, and the postbuckling behavior of such composites approaches the one corresponding to a single column of particle system (see Figure 2d).

Next, we illustrate the role of the inclusion spacing ratio in the soft composite behavior. **Figure 3** presents the instability-induced patterns in the composites with various inclusion spacing ratios $\xi = 0.7$ a), 0.8 b), 0.9 c), 0.95 d), and fixed periodicity aspect ratio $\eta = 3$. The results are shown for the composites with applied strain levels: $\varepsilon = 0.17$ a), 0.15 b), 0.06 c), and 0.04 d). We observe that all composites develop wavy-like patterns, and the length of the wavy-like pattern increases with the increase in inclusion spacing ratio. The wave length of the instability-induced pattern in the composite with $\xi = 0.95$ is significantly larger than the characteristic size of its unit cell, similar to the one shown in Figure 1e; these patterns can be attributed to the transition to the macroscopic or long wave mode. Remarkably, these pattern transformations are fully reversible since the composites restore their initial states after removing the applied load.

The experimental stress–strain curves for the composites with a) various spacing ratios and b) various periodicity ratios are shown in **Figure 4**. Prior to the onset of instability, the composites with larger spacing ratio and/or smaller aspect ratio possess stronger reinforcement and exhibit stiffer responses. When the critical deformation level is achieved, the softening behavior is observed due to the instability-induced microstructure transformations; the softening effect weakens for the composites with smaller spacing ratio and/or larger periodicity aspect ratio. In particular, for the composite with $\xi = 0.7$, $\eta = 3$, only slight softening is observed at $\varepsilon = 0.152$; and for the composite with single column of inclusions (i.e., $\eta = 24$), the softening behavior is barely detectable though the instability can be readily identified from visual observation of the pattern change. Thus, the composite response can be described by two effective convex strain energy functions merged at the onset of instability, and it is characterized by the reduced effective stiffness in the postbuckling regime.

Next, we summarize our numerical predictions together with experimental observations of the dependence of the a) critical strain and b) critical wavenumber as functions of periodicity aspect ratio for the composites with various inclusion

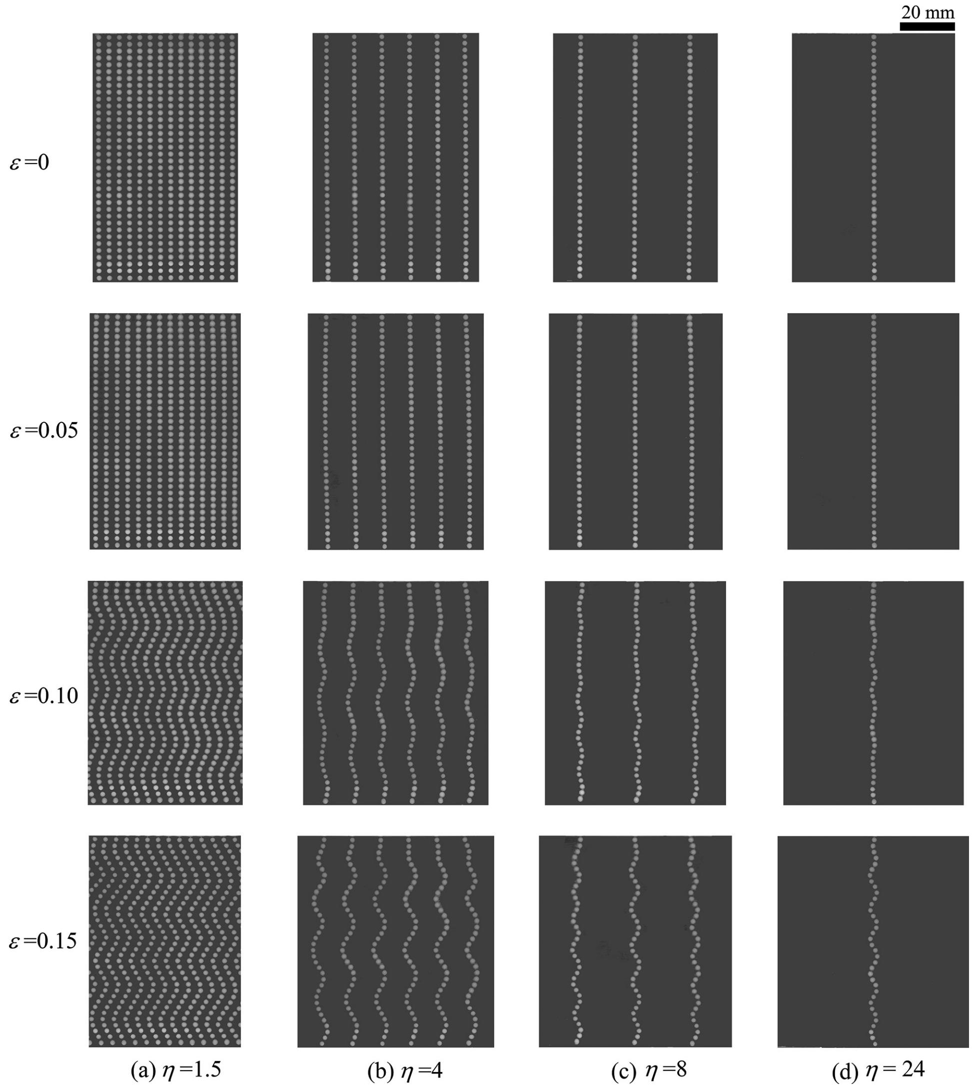

Figure 2. Deformation sequences of the composites with varying periodicity aspect ratios loaded at different deformation levels. The inclusion spacing ratio is fixed as $\xi = 0.8$.

spacing ratios in **Figure 5**. The dotted and continuous curves correspond to the numerically predicted macroscopic and microscopic instabilities, respectively. We use the hollow and filled triangles to denote the experimentally observed critical strains and wavelengths (wavenumbers) corresponding to the numerically detected microscopic and macroscopic

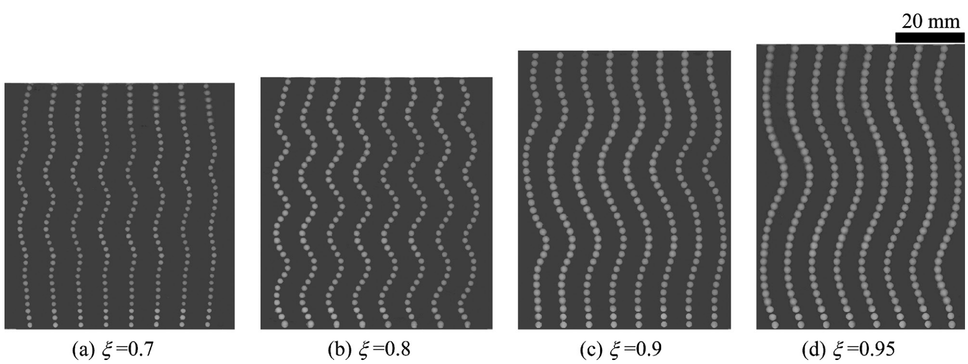

Figure 3. Buckled configurations in soft composites with various inclusion spacing ratios $\xi = 0.7$, 0.8, 0.9, 0.95; and fixed periodicity aspect ratio $\eta = 3$. The results are given at strain levels $\varepsilon = 0.17$ a), 0.15 b), 0.06 c), and 0.04 d).

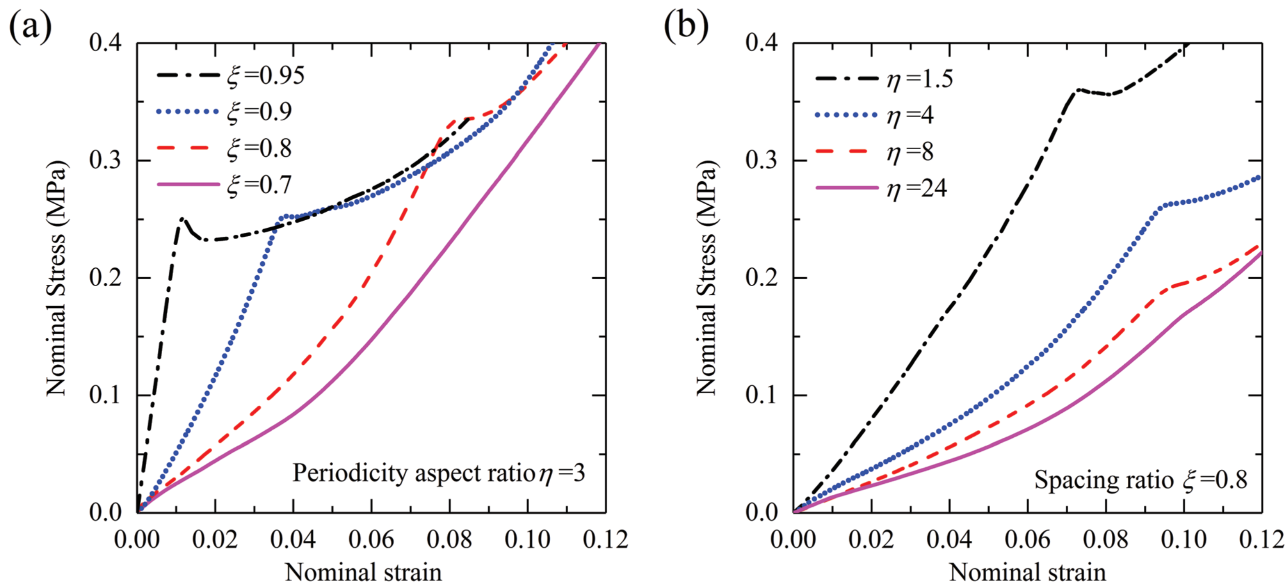

Figure 4. Experimental stress–strain curves for the composites with various spacing ratios a) and various periodicity aspect ratios b).

instabilities, respectively. The experimental critical strain is measured as the deformation level at which the onset of material softening is detected. We observe a qualitative agreement between the numerically predicted trends and experimental results. Interestingly, the domain formation is observed, when the numerical analysis detects the instability at a special limit of the so-called macroscopic instabilities ($k_{cr} \rightarrow 0$). The macroscopic instability analysis can only detect the onset of instabilities; however, it cannot provide the information on the characteristic wavelength of the instability-induced domains. We note, however, the interesting correspondence of the prediction of the macroscopic instabilities and the new domain formations observed in the experiments. We observe that both simulations and experiments indicate that the composites with higher inclusion spacing ratio are more prone to instabilities and buckle earlier (see Figure 5a). The critical strain dependence on the periodicity aspect ratio changes as the spacing ratio is increased. For the composite with small spacing ratio (for example, $\xi = 0.5$), critical strains are found to increase with the increase in the periodicity aspect ratio. When the spacing ratio

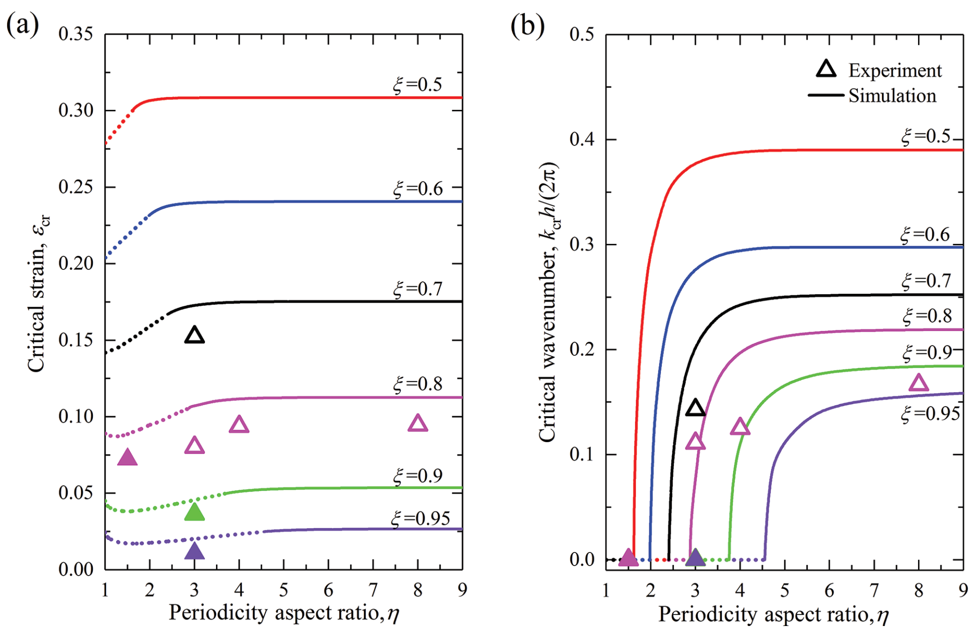

Figure 5. The dependence of critical strain a) and critical wavenumber b) on periodicity aspect ratio for the composites with various spacing ratios. The dotted curves and filled triangular symbols correspond to macroscopic instabilities, while continuous curves and hollow triangular symbols correspond to microscopic instabilities.

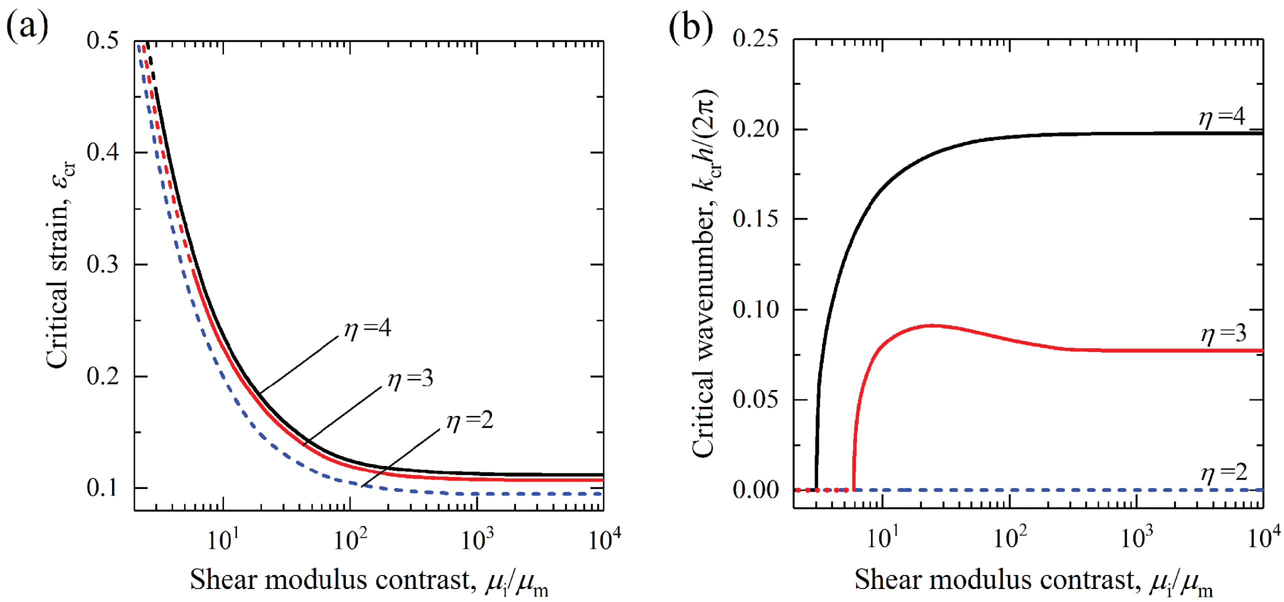

Figure 6. The dependence of critical strain a) and critical wavenumber b) on inclusion-to-matrix shear modulus contrast μ_i/μ_m. The composite spacing ratio is fixed as $\xi = 0.8$. Dotted and continuous curves correspond to macroscopic and microscopic instabilities, respectively.

attains a certain value, the dependence changes and a minimum critical strain is observed at a certain value of periodicity aspect ratio, depending on the inclusion spacing ratio. For example, for the composites with $\xi = 0.9$, the minimum critical strain ($\varepsilon_{cr}^{min} = 0.038$) occurs at $\eta \approx 1.4$. Moreover, we note that the experimental critical strains are observed to be lower than the numerical results. This may be due to various factors, such as the boundary effects for the finite-sized specimens tested in experiments, which are not considered in the numerical simulations for the infinite periodic composites.[24,28,29]

Figure 5b shows the dependence of critical wavenumber on the periodicity aspect ratio for the soft composites with various fixed inclusion spacing ratios. Our simulations predict that the composites with high spacing ratio and/or low periodicity aspect ratio develop macroscopic instability (namely, $k_{cr} \to 0$); these cases correspond to the experimentally observed domain formations. Both experiments and simulations show that an increase in periodicity aspect ratio, or a decrease in inclusion spacing ratio can result in a transition from domain formations to the appearance of periodic wavy chains of particles. Moreover, both critical strain and critical wavenumber are found to be barely influenced by the change in the periodicity aspect ratio when it is large enough ($\eta > 6$ for the composites with inclusion spacing ratio $\xi = 0.8$); this agrees well with our experimental observations for the composites with $\eta = 8$ and 24, showing similar responses (compare Figure 2c,d). These numerical predictions, together with the experimental observations, indicate that the composites with more dense assemblies of the stiff particles tend to develop the twinning domains (upon onset of instabilities); apparently, these patterns are energetically favorable over the wavy patterns in these configurations. Once the distance between the columns of particles is increased, the composites start to exhibit laminate-like buckling behavior—with the effective stiffer layer formed from the column of stiff inclusions—developing the wavy patterns with various wavelengths.

Finally, we numerically examine the influence of the material composition on the composite buckling behavior. **Figure 6** presents the dependence of a) critical strain and b) critical wavenumber on the inclusion-to-matrix shear modulus contrast μ_i/μ_m for the composites with periodicity aspect ratio $\eta = 2$, 3, 4 and fixed spacing ratio $\xi = 0.8$. We observe that the composites with higher shear modulus contrast buckle earlier (at lower strains); interestingly, an increase in the shear modulus contrast may result in the buckling mode switch from macroscopic instability to microscopic instability (see Figure 6b) depending on the initial microstructure parameters. For example, the switch of the buckling mode from macroscopic to microscopic instability occurs at $\mu_i/\mu_m \approx 5.9$ for the composite with periodicity aspect ratio $\eta = 3$ and initial spacing ratio $\xi = 0.8$. In the range of low shear modulus contrasts, the inclusions are able to develop significant deformations, and change their shape resulting in strong stabilization of the composite and in significant changes in the buckling modes developing at large strains.

In conclusion, we have observed experimentally the formation of antisymmetric domains, and the evolution of the instability-induced patterns into periodic wavy chains. These predetermined patterns and transitions are dictated by the initial microstructure geometrical parameters, thus providing the means to tailor the transformative behavior of soft composites and to predesign a variety of switchable functions. The observed domain formation phenomenon in the soft composites can be used for designing materials with switchable functionalities drawn from different length scales. The material design can be further facilitated through numerical computations, as we have shown, the employed numerical method predicts the phenomenon, and can guide towards the desired functionalities achieved through tailored microstructures. We note, however, that the computationally macroscopic instability analysis alone is not enough, and it requires to be accompanied with the full microscopic analysis for the reliable predictions of the domain formations in soft composites. This approach can be combined with the energy convexity consideration along the loading path to identify the energetically preferable post-buckling configurations of the soft composites.[59] We note that the emergence of the domains happens in the composite configurations with dense population of the stiff inclusions. However, when the particle frustration is relaxed—as the distance between the columns of inclusions increases—the composites develop wavy patterns resembling the buckling behavior in soft laminates with the effective stiff layer formed from stiff particle columns. Apparently, the domain patterns are energetically preferable over the wavy patterns in the composite configurations with dense concentration of the stiff inclusions; interestingly, the surface patterns observed in stiff-thin-film/soft-substrate systems show similar behaviors and transitions from twining patterns to wrinkles. Moreover, the formation of the domains in the soft composites is reminiscent of the structures emerging in different systems such as twin patterns in martensitic phase transformations, liquid crystals, and nematic elastomers.

Our findings open new ways for developing the reconfigurable mechanical metamaterials that can find applications in a large variety of fields from acoustic metamaterials, actuators, and soft robotics to morphing devices remotely controlled by external fields for biomedical applications. Thus, for example, the observed switchable behavior can be potentially induced by electric[60] or magnetic[61] fields, or thermally,[62] extending application of the phenomenon in a broad class of architected active materials. Furthermore, these controllable microstructure transformations can be potentially merged at different length scales with other material systems, such as laminates,[63] periodic porous,[28] and bistable structures[64] providing the opportunity for the design of new hierarchical materials that draw their functionalities from different wavelengths.

Supporting Information

Supporting Information is available from the Wiley Online Library or from the author.

Acknowledgements

J.L. and T.D.P. contributed equally to this work. This work was supported by the Israel Science Foundation (Grant Nos. 1550/15 and 1973/15). J.L. thanks the support of Lady Davis graduate student fellowship.

Conflict of Interest

The authors declare no conflict of interest.

Keywords

domain formations, heterogeneous materials, instabilities, pattern transitions

Received: November 11, 2018
Revised: December 26, 2018
Published online: February 14, 2019

[1] S. Shan, S. H. Kang, J. R. Raney, P. Wang, L. Fang, F. Candido, J. A. Lewis, K. Bertoldi, *Adv. Mater.* **2015**, *27*, 4296.
[2] E. Acome, S. K. Mitchell, T. G. Morrissey, M. B. Emmett, C. Benjamin, M. King, M. Radakovitz, C. Keplinger, *Science* **2018**, *359*, 61.
[3] N. Kellaris, V. Gopaluni Venkata, G. M. Smith, S. K. Mitchell, C. Keplinger, *Sci. Rob.* **2018**, *3*, eaar3276.
[4] K. Yu, N. X. Fang, G. Huang, Q. Wang, *Adv. Mater.* **2018**, *30*, 1706348.
[5] Y. Kim, H. Yuk, R. Zhao, S. A. Chester, X. Zhao, *Nature* **2018**, *558*, 274.
[6] C. R. Tipton, E. Han, T. Mullin, *Soft Matter* **2012**, *8*, 6880.
[7] C. Yuan, X. Mu, C. K. Dunn, J. Haidar, T. Wang, H. Jerry Qi, *Adv. Funct. Mater.* **2018**, *28*, 1705727.
[8] C. Yuan, D. J. Roach, C. K. Dunn, Q. Mu, X. Kuang, C. M. Yakacki, T. J. Wang, K. Yu, H. J. Qi, *Soft Matter* **2017**, *13*, 5558.
[9] Z. Zhao, J. Wu, X. Mu, H. Chen, H. J. Qi, D. Fang, *Macromol. Rapid Commun.* **2017**, *38*, 1600625.
[10] Z. Wang, K. Li, Q. He, S. Cai, *Adv. Mater.* **2018**, 1806849.
[11] S. Babaee, N. Viard, P. Wang, N. X. Fang, K. Bertoldi, *Adv. Mater.* **2016**, *28*, 1631.
[12] J. Liu, T. Gu, S. Shan, S. H. Kang, J. C. Weaver, K. Bertoldi, *Adv. Mater.* **2016**, *28*, 6619.
[13] Y. Tang, G. Lin, L. Han, S. Qiu, S. Yang, J. Yin, *Adv. Mater.* **2015**, *27*, 7181.
[14] D. M. Kochmann, K. Bertoldi, *Appl. Mech. Rev.* **2017**, *69*, 050801.
[15] D. W. Lee, J. H. Lee, J. H. Jin, *Compos. Struct.* **2018**, *204*, 487.
[16] X. Guo, X. Wang, D. Ou, J. Ye, W. Pang, Y. Huang, J. A. Rogers, Y. Zhang, *npj Flexible Electron.* **2018**, *2*, 14.
[17] S. Xu, Z. Yan, K. I. Jang, W. Huang, H. Fu, J. Kim, Z. Wei, M. Flavin, J. McCracken, R. Wang, A. Badea, Y. Liu, D. Xiao, G. Zhou, J. Lee, H. U. Chung, H. Cheng, W. Ren, A. Banks, X. Li, U. Paik, R. G. Nuzzo, Y. Huang, Y. Zhang, J. A. Rogers, *Science* **2015**, *347*, 154.
[18] M. Zarek, M. Layani, I. Cooperstein, E. Sachyani, D. Cohn, S. Magdassi, *Adv. Mater.* **2016**, *28*, 4449.
[19] H. Fu, K. Nan, W. Bai, W. Huang, K. Bai, L. Lu, C. Zhou, Y. Liu, F. Liu, J. Wang, M. Han, Z. Yan, H. Luan, Y. Zhang, Y. Zhang, J. Zhao, X. Cheng, M. Li, J. W. Lee, Y. Liu, D. Fang, X. Li, Y. Huang, Y. Zhang, J. A. Rogers, *Nat. Mater.* **2018**, *17*, 268.
[20] D. Krishnan, H. T. Johnson, *J. Mech. Phys. Solids* **2009**, *57*, 1500.
[21] J. R. Raney, N. Nadkarni, C. Daraio, D. M. Kochmann, J. A. Lewis, K. Bertoldi, *Proc. Natl. Acad. Sci. USA* **2016**, *113*, 9722.
[22] P. Wang, F. Casadei, S. Shan, J. C. Weaver, K. Bertoldi, *Phys. Rev. Lett.* **2014**, *113*, 014301.
[23] B. Deng, J. R. Raney, V. Tournat, K. Bertoldi, *Phys. Rev. Lett.* **2017**, *118*, 204102.
[24] J. Li, V. Slesarenko, S. Rudykh, *Soft Matter* **2018**, *14*, 6171.
[25] M. Guttag, M. C. Boyce, *Adv. Funct. Mater.* **2015**, *25*, 3641.
[26] J. T. B. Overvelde, T. Kloek, J. J. A. D'haen, K. Bertoldi, *Proc. Natl. Acad. Sci. USA* **2015**, *112*, 10863.
[27] T. Chen, O. R. Bilal, K. Shea, C. Daraio, *Proc. Natl. Acad. Sci. USA* **2018**, *115*, 5698.
[28] T. Mullin, S. Deschanel, K. Bertoldi, M. C. Boyce, *Phys. Rev. Lett.* **2007**, *99*, 084301.
[29] K. Bertoldi, M. C. Boyce, S. Deschanel, S. M. Prange, T. Mullin, *J. Mech. Phys. Solids* **2008**, *56*, 2642.
[30] B. Florijn, C. Coulais, M. van Hecke, *Phys. Rev. Lett.* **2014**, *113*, 175503.
[31] B. Florijn, C. Coulais, M. van Hecke, *Soft Matter* **2016**, *12*, 8736.
[32] K. Bertoldi, P. M. Reis, S. Willshaw, T. Mullin, *Adv. Mater.* **2010**, *22*, 361.
[33] J. T. B. Overvelde, S. Shan, K. Bertoldi, *Adv. Mater.* **2012**, *24*, 2337.
[34] S. Babaee, J. Shim, J. C. Weaver, E. R. Chen, N. Patel, K. Bertoldi, *Adv. Mater.* **2013**, *25*, 5044.

[35] J. Shim, S. Shan, A. Košmrlj, S. H. Kang, E. R. Chen, J. C. Weaver, K. Bertoldi, *Soft Matter* **2013**, *9*, 8198.
[36] J. Li, J. Shim, J. Deng, J. T. B. Overvelde, X. Zhu, K. Bertoldi, S. Yang, *Soft Matter* **2012**, *8*, 10322.
[37] K. Bertoldi, M. C. Boyce, *Phys. Rev. B* **2008**, *78*, 184107.
[38] P. Wang, J. Shim, K. Bertoldi, *Phys. Rev. B* **2013**, *88*, 014304.
[39] S. Shan, S. H. Kang, P. Wang, C. Qu, S. Shian, E. R. Chen, K. Bertoldi, *Adv. Funct. Mater.* **2014**, *24*, 4935.
[40] J. Shim, P. Wang, K. Bertoldi, *Int. J. Solids Struct.* **2015**, *58*, 52.
[41] D. Yang, B. Mosadegh, A. Ainla, B. Lee, F. Khashai, Z. Suo, K. Bertoldi, G. M. Whitesides, *Adv. Mater.* **2015**, *27*, 6323.
[42] R. W. Ogden, *Non-Linear Elastic Deformations*, Dover Publications, New York **1997**.
[43] J. Merodio, R. W. Ogden, *Int. J. Solids Struct.* **2003**, *40*, 4707.
[44] J. Merodio, R. W. Ogden, *Q. Appl. Math.* **2005**, *63*, 325.
[45] N. Triantafyllidis, B. N. Maker, *J. Appl. Mech.* **1985**, *52*, 794.
[46] G. Geymonat, S. Müller, N. Triantafyllidis, *Arch. Ration. Mech. Anal.* **1993**, *122*, 231.
[47] C. Gao, B. P. J. Hasseldine, L. Li, J. C. Weaver, Y. Li, *Adv. Mater.* **2018**, *30*, 1800579.
[48] S. Singamaneni, K. Bertoldi, S. Chang, J. H. Jang, S. L. Young, E. L. Thomas, M. C. Boyce, V. V. Tsukruk, *Adv. Funct. Mater.* **2009**, *19*, 1426.
[49] V. Slesarenko, S. Rudykh, *J. Mech. Phys. Solids* **2017**, *99*, 471.
[50] J. M. Ball, R. D. James, *Arch. Ration. Mech. Anal.* **1987**, *100*, 13.
[51] K. Bhattacharya, *Microstructure of Martensite: Why It Forms and How It Gives Rise to the Shape–Memory Effect*, Oxford University Press, New York **2003**.
[52] L. M. Blinov, *J. Phys., Colloq.* **1979**, *40*, 247.
[53] L. Tran, M. O. Lavrentovich, G. Durey, A. Darmon, M. F. Haase, N. Li, D. Lee, K. J. Stebe, R. D. Kamien, T. Lopez-Leon, *Phys. Rev. X* **2017**, *7*, 041029.
[54] A. DeSimone, G. Dolzmann, *Phys. D* **2000**, *136*, 175.
[55] S. Conti, *J. Mech. Phys. Solids* **2002**, *50*, 1431.
[56] X. Chen, J. W. Hutchinson, *J. Appl. Mech.* **2004**, *71*, 597.
[57] S. Cai, D. Breid, A. J. Crosby, Z. Suo, J. W. Hutchinson, *J. Mech. Phys. Solids* **2011**, *59*, 1094.
[58] J. Yin, J. L. Yagüe, D. Eggenspieler, K. K. Gleason, M. C. Boyce, *Adv. Mater.* **2012**, *24*, 5441.
[59] J. Furer, P. Ponte Castañeda, *J. Mech. Phys. Solids* **2018**, *118*, 98.
[60] Z. Zheng, R. S. Zola, H. K. Bisoyi, L. Wang, Y. Li, T. J. Bunning, Q. Li, *Adv. Mater.* **2017**, *29*, 1701903.
[61] W. Wang, J. V. I. Timonen, A. Carlson, D. M. Drotlef, C. T. Zhang, S. Kolle, A. Grinthal, T.-S. Wong, B. Hatton, S. H. Kang, S. Kennedy, J. Chi, R. T. Blough, M. Sitti, L. Mahadevan, J. Aizenberg, *Nature* **2018**, *559*, 77.
[62] Z. Zhao, X. Kuang, C. Yuan, H. J. Qi, D. Fang, *ACS Appl. Mater. Interfaces* **2018**, *10*, 19932.
[63] G. W. Milton, *J. Mech. Phys. Solids* **1992**, *40*, 1105.
[64] K. Che, C. Yuan, H. J. Qi, J. Meaud, *Soft Matter* **2018**, *14*, 2492.